Angle-resolved photoemission study of $AuGa_2$ and $AuIn_2$ intermetallic compounds

Jeffrey G. Nelson, W. J. Gignac, Sehun Kim, Jeffrey R. Lince, and R. Stanley Williams
Department of Chemistry and Biochemistry, University of California, Los Angeles, Los Angeles, California 90024
(Received 17 August 1984)

The (001) surfaces of $AuGa_2$ and $AuIn_2$ intermetallic compounds were studied with use of synchrotron-radiation-excited angle-resolved photoemission. Spectra collected for photoelectron emission normal to the sample surfaces were used to map the E versus $\mathbf{k}$ dispersion relation of both compounds along the Δ symmetry line of the bulk Brillouin zone. The results show that the Au $5d$ bands of each compound are relatively flat, but the splittings of the bands at point Γ are nearly the same as for elemental Au. A surface state was also observed on each surface in a band-gap region about 6 eV below the Fermi levels of the two compounds.

I. INTRODUCTION

Au, $AuGa_2$, and $AuIn_2$ form an interesting series of metals for the study of the Au $5d$ orbitals in solids. In elemental Au, the atoms reside on a face-centered cubic (fcc) lattice with a nearest-neighbor distance of 2.88 Å. $AuGa_2$ and $AuIn_2$ have the fluorite structure, in which the Au atoms form an fcc sublattice where each Au atom is at the center of a cube with eight group-III (Ga or In) atoms situated at the corners. In this arrangement, the Au-Au nearest-neighbor distances are 4.29 and 4.60 Å for $AuGa_2$ and $AuIn_2$, respectively. The strength of the interaction between the $5d$ orbitals on neighboring Au atoms in this group should decrease dramatically with increasing atomic separation and should be evident as a narrowing in the d-band structure of these metals. Examining the energy bands of these materials at the Γ point of the Brillouin zone (BZ), where each band reduces to a single type of atomic l character, will provide interesting information about the Au d-d interactions as a function of primarily interatomic distance.

Au is an extremely well-studied material, but most previous investigations of the electronic structure of the Au(group III)$_2$ intermetallic compounds have been limited to optical reflectivity measurements,[1] Fermi-surface determinations,[2,3] and total valence-band density-of-states measurements.[4–6] The results of van Attekum *et al.*[6] show that the total Au $5d$-band width, as measured using x-ray photoelectron spectroscopy (XPS) of polycrystalline samples, decreases in the series Au, $AuGa_2$, and $AuIn_2$. More recently, the surface net and electronic structure of the $AuGa_2(001)$ single-crystal surface have been studied using low-energy electron diffraction (LEED), Auger-electron spectroscopy (AES), and electron-energy-loss spectroscopy,[7] in preparation for more detailed investigations of the electronic band structure.

Angle-resolved photoelectron spectroscopy (ARPES) has proved to be an effective technique for studying the electronic structure of single-crystal materials by providing information about the E versus $\mathbf{k}$ dispersion relation along specific directions in the BZ.[8–10] This technique is well suited to measure the binding energies of the Au $5d$ levels at various points in the BZ, which is necessary to study the Au $5d$-$5d$ interactions in the Au, $AuGa_2$, $AuIn_2$ series. This type of detailed electronic structure measurement has not previously been applied to these intermetallic compounds.

Switendick and Narath[11] have calculated nonrelativistic augmented-plane-wave (APW) band structures for $AuAl_2$, $AuGa_2$, and $AuIn_2$. These calculations show a marked narrowing in the d bands of $AuIn_2$ compared to $AuGa_2$. Both the splitting of the bands at Γ and the band dispersion as $\mathbf{k}$ varied outward to the BZ boundaries were much smaller for $AuIn_2$. However, the total width of the calculated d bands was much smaller than indicated by the XPS valence-band spectra[6] of both compounds. Since the calculations neglected spin-orbit splitting, which should be large in Au $5d$ orbitals, this last observation is perhaps not surprising.

In order to assist in understanding the d-band structure of $AuGa_2$ and $AuIn_2$, a mixed-basis band-structure interpolation scheme including spin-orbit splitting was developed.[12] The interpolation scheme was first fitted to the APW calculations, and then the parameters were adjusted to improve the agreement between the ARPES and the calculated bands at Γ. In this way, semiempirical band structures for both $AuGa_2$ and $AuIn_2$ were constructed, which enabled the symmetries of valence bands to be determined, and helped with the interpretation of all the ARPES spectra.

The focus of this paper will be on mapping the band structure of $AuGa_2$ and $AuIn_2$ along Δ using normal-emission ARPES from (001) surfaces of single crystals. From the results of the experimental bulk band structures at Γ, the "crystal-field" (Δ) and the spin-orbit (ξ) parameters for the Au, $AuGa_2$, and $AuIn_2$ series were calculated in order to look at the Au $5d$-$5d$ interactions as a function of interatomic distance. A surface state was also observed on both surfaces inside a band-gap region of the d bands along the Δ symmetry axis of the BZ. Section II will describe the experimental procedure followed in this work, while Sec. III presents the results of the ARPES experiments on $AuGa_2$ and $AuIn_2$. A discussion of the findings of this work and their relationship to previous studies appears in Sec. IV.

II. EXPERIMENTAL PROCEDURE

The experiments were performed on beam line I-2 (the 8° port) at the Standford Synchrotron Radiation Laborato-

ry (SSRL). All ARPES measurements were made in an ultrahigh vacuum analysis chamber provided by SSRL with a base pressure of 6×10^{-10} Torr. The chamber was equipped with a single-axis sample manipulator, LEED optics, and a Vacuum Generators, Ltd. (VG) ADES 400 angle-resolving photoelectron spectrometer that had an acceptance cone half-angle of $\sim3°$. Both samples were mounted such that the plane of incidence of the photon beam contained the polarization vector of the radiation (p polarized) and the [110] axis of the crystals. Both normal and off-normal emission spectra were collected with the photon beam 45° from the [001] axis of the samples. A single spectrum required approximately 7 min to collect in order to ensure that there were a minimum of 3000 counts in the strongest feature of each spectrum. The storage ring (SPEAR) was typically operating with a beam energy of 3.0 GeV and a current of between 30 and 60 mA. Photon energies in the range of 14—32 eV were used, and the total analyzer plus monochromator energy resolution was better than 0.2 eV in all cases. All of the ARPES data were collected with the sample at room temperature.

The energy distribution curves (EDC's) were collected as a function of photoelectron kinetic energy. In order to determine a reference binding energy for all the spectra, a Fermi level (E_F) was assigned to spectra that were the sums of all ARPES spectra collected at each photon energy, in order to include initial states from a reasonably large portion of the BZ. This was accomplished by establishing a baseline for each summed spectrum, and then defining E_F to be the energy where the EDC's crossed a line that was half the distance from the baseline to a second line that was fitted to the flat s-p plateau of that EDC's.

The procedure for the preparation of the $AuGa_2$ and $AuIn_2$ crystal surfaces used in this study has been described in detail elsewhere.[7,13] Both crystal surfaces were oriented to within 1° of the (001) plane using Laue x-ray diffractometry. The earlier study showed that in the case of $AuGa_2$, after alternating cycles of argon-ion bombardment at energies from 3 keV to 500 eV and annealing to 575 K, a sharp LEED pattern, which was interpreted in terms of two perpendicular domains with a $(\sqrt{2}\times\sqrt{18})R45°$ reconstruction, was seen. This same surface reconstruction was also observed for $AuIn_2(001)$ in this study. Although AES measurements were not available during the ARPES experiments, sharp LEED spots with no streaking or splitting and the absence of photoemission features in the valence band caused by oxygen or carbon indicated that both samples were free of contamination.

III. RESULTS

Figure 1 shows a set of normal-emission ARPES spectra that were collected from the $AuGa_2(001)$-$(\sqrt{2}\times\sqrt{18})R45°$ reconstructed surface. Various sets of features have been connected with lines and labeled A—G. Of these features, only two (A and B) show substantial dispersion as the photon energy is increased. The peaks labeled A correspond to photoemission from an s-p band that rises steeply between Γ and X, crossing the Fermi level before reaching Γ. Feature B is only seen at low

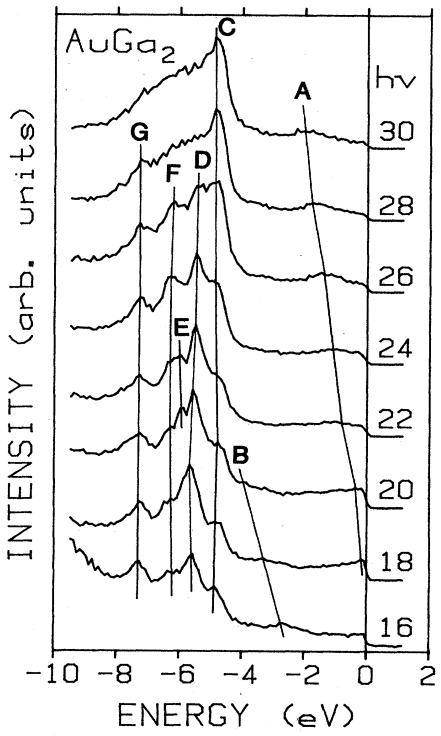

FIG. 1. ARPES spectra of clean $AuGa_2(001)$-$(\sqrt{2}\times\sqrt{18})R45°$ taken at normal emission with the sample at room temperature. The line labeled A shows the peaks that have been assigned to transitions from the second s-p band of $AuGa_2$. Features B and E have been assigned to a surface umklapp process. Lines C, D, and G indicate bulk transitions from the Au $5d$ spin-orbit split levels. Finally, the peaks labeled F, which lie in a band gap in $AuGa_2$ along Δ, have been assigned to a surface state.

photon energies (16—20 eV). These two sets of features are broader than the others through the entire range of photon energies used in this experiment. The other five features show relatively little dispersion, which is indicative of d bands (in this case, mostly Au $5d$ in character).

ARPES spectra were also collected after the $AuGa_2$ sample was exposed to ~180 L of O_2. The feature labeled F was much more sensitive to this contamination than any of the other features, in that a small amount of adsorbed oxygen was sufficient to reduce the intensity of feature F to below a detectable limit. Off-normal ARPES spectra of the clean surface were collected in order to observe the dispersion of any features with the parallel component of momentum ($k_{||}$). Feature F was the only peak in the d-band region to exhibit noticeable dispersion of this type.

Figure 2 consists of a set of normal-emission spectra from the (001)-$(\sqrt{2}\times\sqrt{18})R45°$ surface of $AuIn_2$. Features are once again connected and labeled A—E. These spectra are less complicated than those of $AuGa_2$, since the features corresponding to B and E in Fig. 1 are missing. However, the $AuIn_2$ spectra show even more clearly the dispersion of the s-p band (feature A). The other four features (labeled B—E) apparently correspond to Au $5d$—like bands. Feature D in the $AuIn_2$ spectra

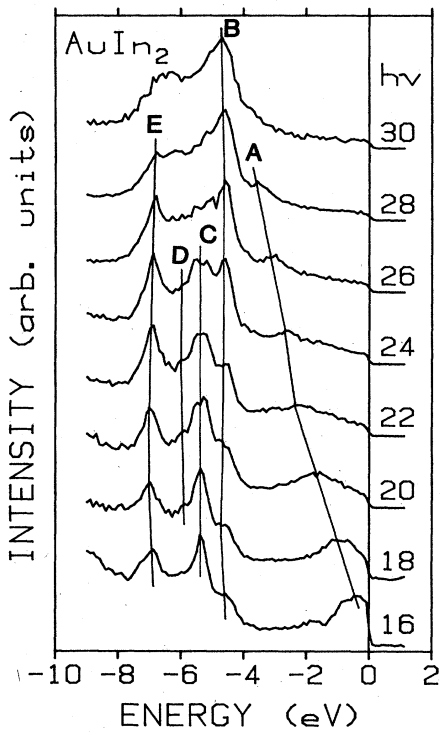

FIG. 2. ARPES spectra of clean $AuIn_2(001)$-$(\sqrt{2}\times\sqrt{18})R45°$ taken at normal emission with the sample at room temperature. The line labeled A shows peaks that have been assigned to transitions from the second s-p band of $AuIn_2$. Features B, C, and E correspond to the $5d$ bands, and D arises from surface-state emission.

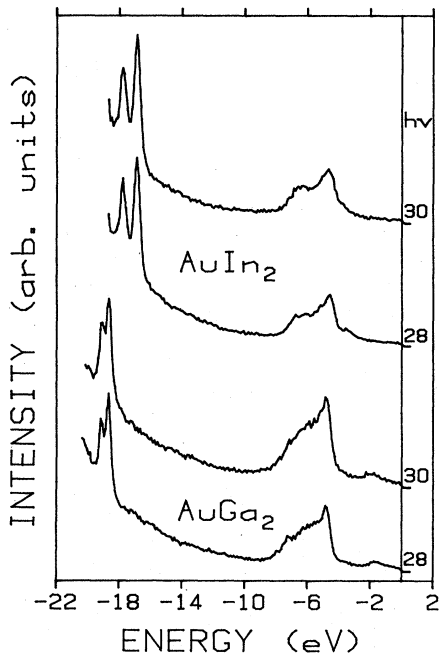

FIG. 3. ARPES spectra of clean $AuGa_2$ and $AuIn_2$ that extend to higher binding energies to reveal the Ga $3d$ and In $4d$ levels.

TABLE I. Binding energies of Ga $3d$ and In $4d$ levels. All values in eV. Estimated uncertainty is 0.1 eV.

	Ga $3d_{5/2}$	Ga $3d_{3/2}$	Spin-orbit splitting
GaAs[a]	18.60	19.04	0.44
GaSb[a]	18.70	19.13	0.43
$AuGa_2$[b]	18.60	19.19	0.59
	In $4d_{5/2}$	In $4d_{3/2}$	Spin-orbit splitting
In metal[c]	16.74	17.64	0.90
InSb[d]	16.71	17.65	0.84
$AuIn_2$[b]	16.83	17.74	0.90

[a]D. E. Eastman, T. C. Chaing, P. Heilmann, and F. J. Himpsel, Phys. Rev. Lett. **45**, 656 (1980). (Binding energy relative to valence-band maximum.)
[b]This work (binding energy relative to Fermi level).
[c]R. A. Pollack, S. P. Kowalczvk, L. Ley, and D. A. Shirley, Phys. Rev. Lett. **29**, 274 (1972). (Binding energy relative to Fermi level.)
[d]L. Ley, R. A. Pollack, F. R. McFeely, S. P. Kowalczyk, and D. A. Shirley, Phys. Rev. B **9**, 600 (1974). (Binding energy relative to Fermi level.)

dispersed in energy with varying $k_{||}$ in a manner very similar to that of feature F in the $AuGa_2$ spectra.

Figure 3 contains a set of two spectra for each compound, which clearly show the sharp spin-orbit split d levels of Ga($3d$) and In($4d$). Table I lists the binding energies and the spin-orbit splittings for Ga $3d$ and In $4d$ for the Au intermetallic compounds compared with other materials. The binding energies for the Ga $3d$ or In $4d$ levels in each series of materials agree with one another to within 0.1 eV, which demonstrates that chemical shifts in these systems are small. The core levels shown in Fig. 3 also indicate the total energy resolution of the ARPES spectra.

IV. DISCUSSION

The data were analyzed using the direct-transition model. The momentum component parallel to the surface ($k_{||}$) is conserved during the exit of the photoelectron through the surface. The normal momentum ($k_{\perp}$) is changed during the exit since the photoelectron has to cross an energy barrier. Since neither the conduction-band structure nor the wave vector of the photoemitted electron are known in advance, **k** of the photoemitted electron *inside* the solid must be estimated. Assuming a free-electron conduction-band structure (i.e., plane-wave final states), the normal component of the photoemitted electron momentum inside the crystal ($k_{\perp,\text{in}}$) is given by

$$k_{\perp,\text{in}}^2=\frac{2m}{\hbar^2}\left[\frac{m^*}{m}(E_k+V_0)-E_k\sin^2\theta\right], \quad (1)$$

where E_k is the kinetic energy of the photoelectron in the vacuum, θ is the polar angle of emission with respect to the sample normal, V_0 is the inner potential, which is assumed to be independent of kinetic energy, and m^* is the

effective mass of the photoelectron. The values of the inner potential used for $AuGa_2$ and $AuIn_2$ were estimated to be 11.16 and 11.41 eV, respectively, which were taken to be the difference between the muffin-tin zero of energy in the APW calculations[11] and the vacuum level as determined from the work functions of the two compounds. The experimental band structure along the Δ line was then found by plotting the binding energy of the photoelectron (relative to the Fermi level) versus $k_\perp$ determined using Eq. (1), for various values of m^*. These plots were then compared to the nonrelativistic band structures of Switendick and Narath,[11] but the agreement was poor for all values of m^*, especially with respect to the d bands.

Whenever the direct-transition model is used to interpret ARPES data, the limitations of the model must be considered in order to assess the level of agreement between theory and experiment. More specifically, situations that lead to the breakdown of momentum selection rules and result in uncertainty in $\mathbf{k}$ must be examined. The effect of the inherent angular and energy resolution of the electron analyzer, the crystal momentum broadening of the photoelectron final states that results from finite mean-free-path lengths,[14] and any broadening attributable to the Debye-Waller factors of the system must be carefully evaluated.[15]

Due to the dispersion of the initial-state bands, changes in the momentum-space region sampled in ARPES can cause very large changes in the observed photoelectron energy distribution curves (EDC's). The actual energy width of features observed in ARPES spectra depends upon both the resolution with which final momentum states are sampled and the energy dispersion of the initial-state bands. This effect is quite evident in Fig. 2, where the s-p band at low binding energy is much broader than the d-level bands at higher binding energy. In general, s-p bands disperse much more rapidly than the almost flat d bands, thus accounting for the relative width of the features seen in the ARPES spectra.

The volume of the crystal momentum space sampled in an ARPES spectrum depends primarily upon the angular resolution of the electron analyzer and the crystal momentum broadening in the photoemission final state. The angular and energy resolution discussed in Sec. II result in an instrumental broadening of $k_\perp$ of 0.23 Å^{-1}, or 11% of the BZ dimensions. The broadening due to the final-state width is inversely proportional to the photoelectron mean free path (l) and the angle (θ) between the momentum vector and the surface normal.[16] Using the inelastic mean free path formula of Seah and Dench,[17] and assuming an average photoelectron kinetic energy of 20 eV, the electron mean free path of $AuGa_2$ and $AuIn_2$ is calculated to be 6.8 Å. Thus the expected $k_\perp$ broadening is 0.30 Å^{-1} in both $AuGa_2$ and $AuIn_2$, which agrees well with the observed uncertainty in the momentum (0.31 Å^{-1}) estimated from the full width at half maximum (FWHM) of the s-p photoemission peak A of $AuIn_2$ in Fig. 2, and the E versus $\mathbf{k}$ dispersion of the calculated Δ_1 valence band.[11] This value corresponds to a final-state FWHM momentum broadening which is 15% of the BZ dimensions. The total volume of $\mathbf{k}$ space sampled in each spectrum of the present ARPES measurements caused by the angular resolution of the analyzer and the uncertainty in $k_\perp$ may be estimated as a cylinder with a volume of 0.015 Å^{-3}, which corresponds to 0.3% of the volume of the BZ. Although this may appear to be a rather small sampling volume of momentum space, it is responsible for the broad photoemission peaks from s-p—like bands.

The last important broadening mechanism to be considered is thermal broadening due to indirect or phonon-assisted transitions. Such contributions to the uncertainty in momentum can best be estimated by looking at the Debye-Waller factors for each system. The bulk Debye temperatures of $AuGa_2$ and $AuIn_2$ are 196 and 187 K, respectively.[18] A rough estimate of the mean-squared vibrational amplitude of each atom in the compounds was obtained using average atomic masses of 112.1 ($AuGa_2$) and 142.2 ($AuIn_2$) and the bulk Debye temperatures. The resulting values of the Debye-Waller factor for $AuGa_2$ and $AuIn_2$ are 0.84 and 0.88, respectively. These numbers represent a modest contribution ($\sim$15%) of indirect transitions to the spectra and show that the direct-transition model is still justified in these systems. To reduce the effect of lattice vibrations on the spectra, the samples could be cooled to liquid-nitrogen temperatures, at which the Debye-Waller factors would be approximately 0.96 ($AuGa_2$) and 0.97 ($AuIn_2$). To appreciably improve the spectra, the sampling volume of momentum space would also have to be decreased substantially by using an ARPES analyzer with much better angular resolution and higher photon energies to increase the mean free paths of the photoelectrons.

Although not negligible, the momentum broadening effects discussed above are not serious enough to invalidate the direct-transition model as applied to the photoemission spectra of $AuGa_2$ and $AuIn_2$. Thus the disagreement between the theoretical APW bands[11] and the experimentally determined bands is largely the result of the inaccuracies in the calculation. One major omission in the APW calculation was neglect of spin-orbit coupling,[11] which should be relatively large for Au 5d orbitals. Also, the binding-energy positions with respect to E_F of the centroids of the d bands were overestimated by about 1 eV, and the d-band widths (even discounting the neglect of spin-orbit effects) were severely underestimated.[12]

In order to obtain a better theoretical estimate of the d bands in $AuGa_2$ and $AuIn_2$, a mixed-basis interpolation scheme including spin-orbit splitting was developed for fluorite structure compounds.[12] The nonrelativistic APW bands of $AuGa_2$ and $AuIn_2$ were fitted using this procedure. Then, using an estimate of the binding energies of the d bands at Γ obtained from the direct-transition model with $m^*=1.0$ and the most intense photoemission features, the parameters of the interpolation scheme were adjusted to produce the three d bands at Γ that agreed with those from the ARPES measurements. Next, the energy bands calculated from the ARPES spectra for various m^* values were compared with the interpolated bands, and reasonable agreement was found for $m^*=1.25$. In principle, an iterative procedure could have been used in which a new set of binding energies for the d bands at Γ would be determined for the new m^* value.

However, for $AuGa_2$ and $AuIn_2$, the d bands were so flat that this was not necessary.

Figure 4(a) shows the energy bands of Au calculated by the interpolation scheme, using parameters from Ref. 12, as well as the interpolated and experimentally determined bands of $AuGa_2$ and $AuIn_2$. By comparing Figs. 4(a), 4(b), and 4(c), one can see that the splitting of the Au $5d$ levels at Γ is almost identical in each case, though the absolute binding energies are somewhat different. The spacing of the Au $5d$ bands can be used to determine the crystal-field (Δ) and the spin-orbit (ξ) parameters in the manner of Wehner *et al.*[10] These parameters, which are only meaningful at Γ, where the crystal momentum is zero, can be used to compare the relative strengths of d-orbital interactions and the spin-orbit coupling. Using the energy eigenvalues calculated by Ballhausen,[19] ξ and Δ

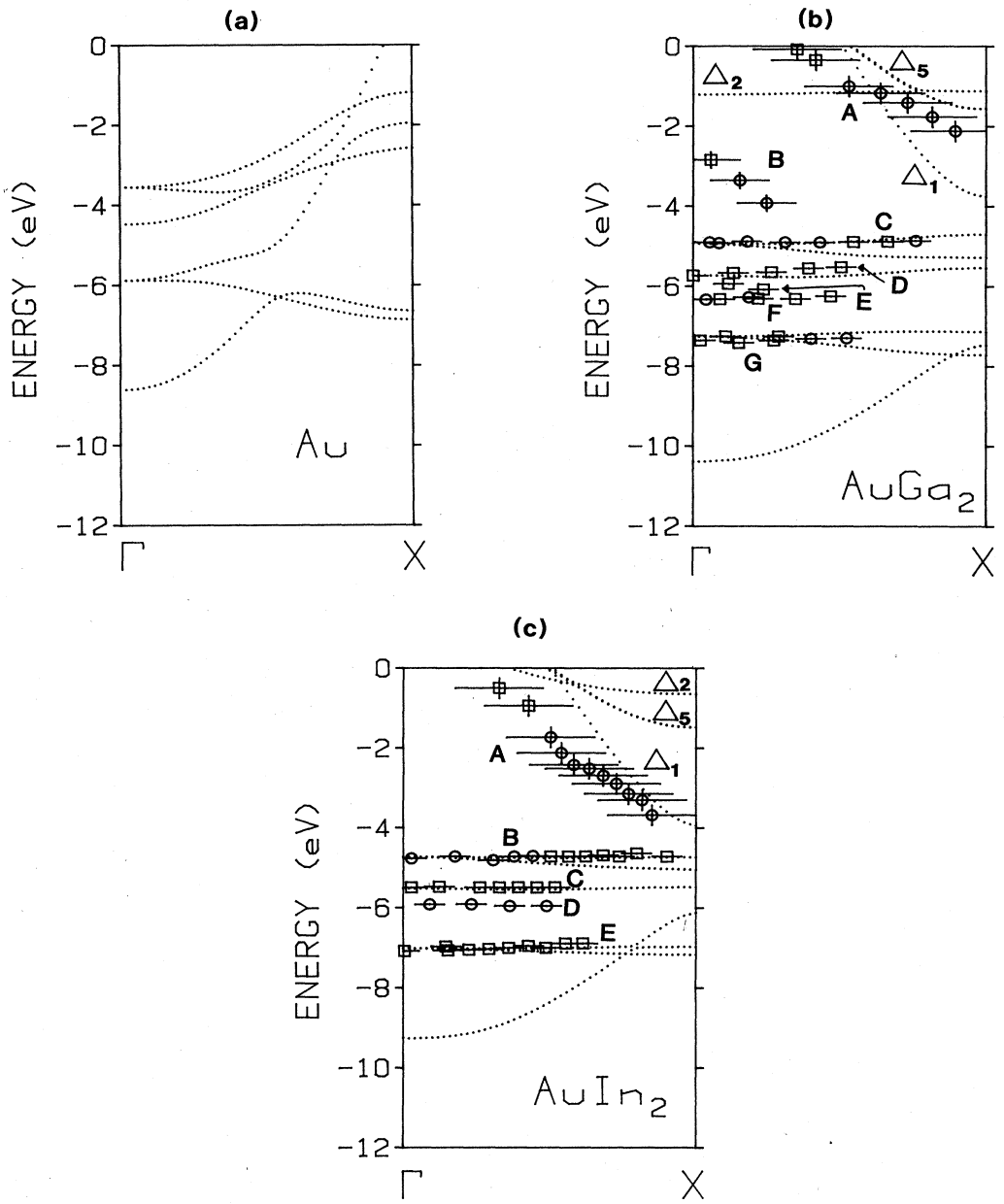

FIG. 4. (a) Band structure of elemental Au along Δ of the fcc-lattice Brillouin zone. The bands were calculated using an interpolation scheme that will be described in detail elsewhere (Ref. 12). The parameters used in this calculation were determined from the position of the Au $5d$ bands at Γ as estimated from the normal-emission ARPES data of Refs. 20 and 21. (b) Band structure of $AuGa_2$ along Δ. The dotted lines were calculated by the same interpolation scheme that was used for elemental Au. The initial-state assignments of the photoemission transitions are shown as squares or circles corresponding to strong or weak features in the spectra of Fig. 1, respectively. For symbols where there are no vertical lines indicating the energy uncertainty in locating a peak in the ARPES spectrum, the height of the symbol corresponds to or exceeds the uncertainty in the measurement. (c) Same as (b), except for $AuIn_2$. The squares and circles represent peaks in the spectra of Fig. 2.

can be extracted from the ARPES data and compared to the same parameters for elemental Au. Table II consists of experimental and theoretical determinations of Δ and ξ for the series Au, $AuGa_2$, and $AuIn_2$.

In the case of Au, previous experiments[20,21] determined a Δ value of 1.22 eV and a spin-orbit parameter of 0.71 eV, which are in good agreement with the same parameters extracted from theoretical band structures.[22] However, the experimental values of Δ for $AuGa_2$ and $AuIn_2$ are much larger than the nonrelativistic d-band splitting calculated by Switendick and Narath,[11] and are essentially identical to one another, whereas the APW calculations predicted a substantial decrease in Δ for $AuIn_2$ with respect to $AuGa_2$. This observation is very surprising, since the Au d-d overlap integrals which give rise to the splittings at Γ (in the linear combination of atomic orbitals sense of Slater and Koster[23]) should decrease dramatically in the series Au, $AuGa_2$, and $AuIn_2$ (as the APW results predict[11]). The large crystal-field effect in the intermetallic compounds may arise from interactions of the Au $5d$ orbitals with the d orbitals of the group III metals (Ga $3d$ or In $4d$). The Au $5d$ bands of $AuAl_2$ should be mapped in detail to test this hypothesis. Since Al has no occupied d orbitals, one might expect the crystal-field splitting to be much smaller for $AuAl_2$ than for $AuGa_2$ or $AuIn_2$. In fact, the total width of the $AuAl_2$ d bands is smaller than for $AuGa_2$, as shown in the valence-band XPS spectra.[6] The spin-orbit parameter, which should essentially be a property only of the Au $5d$ orbitals, is very similar for all three systems.

The width of the d bands of Au is broadened considerably by mixing with the lowest-energy plane-wave band, as shown in Fig. 4(a). Since the lattice constant of $AuGa_2$ and $AuIn_2$ are so much larger than for Au, the BZ dimensions are much smaller. In the case of the two intermetallic compounds, the plane-wave band reaches the BZ boundary at X before it can cross the d bands, as shown in Figs. 4(b) and 4(c). Thus the d bands of $AuGa_2$ and $AuIn_2$ essentially reside within a band gap in the plane-wave bands, and do not mix with the highly dispersing state. This allows the d-band width of the Au density of states to be much larger than for $AuGa_2$ and $AuIn_2$, even though the d-band splitting at Γ is nearly the same for all three materials.

In addition to the conservation of momentum conditions, there exist uniquely solid-state selection rules in ARPES that deal with final states observed along symmetry directions.[24] Since an ARPES experiment chooses a particular final state (which has particular symmetry properties), the initial states that may be sampled are determined by the radiation polarization with respect to the crystalline axes of the sample. In the case of normal photoemission from a (001) surface of a crystal with T_d symmetry and ignoring relativistic effects, the final-state symmetry must be Δ_1 in order for the photoemitted electron to reach the detector. This requires the initial state to have either Δ_5 or Δ_1 symmetry,[24] both of which are allowed by the experimental geometry chosen for this experiment. These symmetry selection rules are only rigorous for detection systems with infinitely good angular resolution, but they provide a basis for analysis of ARPES with good angular resolution.

These selection rules will be used in analyzing photoemission from the s-p valence bands that reside to the lower binding energy side of the d bands, since spin-orbit effects were not included in the interpolation scheme for the s-p bands. Feature A in the $AuGa_2$ spectra (Fig. 1) is caused by transitions from an s-p band between Γ and X. Unfortunately, its position with respect to the calculated bands [Fig. 4(b)] is such that it is not possible to determine if the transition originates from a Δ_1 or Δ_5 initial state, since the experimental points essentially fall between two calculated bands. Photoemission from the flat Δ_2 band is not allowed by the selection rule, and in fact no peak corresponding to this band is observed in any of the ARPES spectra. This observation is actually somewhat surprising, since the selection rules are not expected to be completely rigorous, and the flat band should yield an extremely high density of initial states to be sampled.

The $AuGa_2$ features labeled B, which only appear at photon energies between 16 and 20 eV, are the result of a surface umklapp process from a region of the BZ with the form: $\mathbf{k}=(\frac{1}{3},\frac{1}{3},x)$. There exists a surface reciprocal-lattice vector $\mathbf{g}=(-\frac{1}{3},-\frac{1}{3},0)$ arising from the $(\sqrt{2}\times\sqrt{18})R45°$ reconstructed surface which has the correct magnitude and direction to diffract photoelectrons emitted from initial states in this region of the BZ to the direction $(0,0,x)$, which can reach the electron-energy analyzer in the normal-emission geometry. Peaks labeled E are also a result of this same umklapp process. These

TABLE II. Binding energies of Au $5d$ levels at Γ. All values in eV. Estimated uncertainty in the experimental binding energies is 0.1 eV.

	Lattice constant (Å)		$E(\Gamma_8^1)$	$E(\Gamma_7)$	$E(\Gamma_8^2)$	Δ	ξ
Au metal	4.08	Expt.[a]	−3.55	−4.45	−5.90	1.23	0.71
		Theor.[b]	−3.38	−4.33	−5.75	1.28	0.70
$AuGa_2$	6.06	Expt.[c]	−4.92	−5.68	−7.31	1.07	0.78
		Theor.[d]	−6.88	−7.60	−7.60	0.72	
$AuIn_2$	6.50	Expt.[c]	−4.72	−5.48	−7.05	1.06	0.75
		Theor.[d]	−6.47	−6.94	−6.94	0.47	

[a]Ref. 20.
[b]Ref. 22.
[c]This work.
[d]Ref. 11.

assignments have been confirmed by generating the valence bands along $\mathbf{k}=(\frac{1}{3},\frac{1}{3},x)$ in the BZ using the interpolation scheme and observing that valence bands exist with the correct binding energies and values of $\mathbf{k}$. Features C, D, and G in the $AuGa_2$ spectra have been assigned to the three d levels that have symmetries (using relativistic notation) of Γ_8^+, Γ_7^+, and Γ_8^+, respectively. The d bands are fairly flat, dispersing only a small amount between Γ and X, especially when compared to the corresponding d bands of Au. The agreement between the dispersion of the interpolated and three experimental d bands that were mapped out assuming a plane-wave final state with $m^*=1.25$ is qualitatively correct, but differences of a few tenths of an eV exist as the bands approach X.

The final feature in the ARPES spectra is in a d-band gap along Δ in $AuGa_2$. Feature F, which has a binding energy of ~ 6.2 eV, lies between the lower Γ_8^+ and Γ_7^+ d levels. These peaks show no dispersion as the photon energy is increased from 16 to 30 eV. In addition, these features are more sensitive to surface contamination than photoemission peaks assigned to bulk bands. Lastly, some dispersion was seen in this feature as the parallel component of the wave vector was increased from zero by moving the detector off-normal. As the polar angle of emission (θ) was increased, the direction of rotation was in the plane containing the [001] and [110] axes. This is equivalent to simultaneously rotating from Γ to J and Γ to J' in the rectangular surface BZ, shown in the inset of Fig. 5, since the surface reconstruction is assumed to contain two perpendicular domains in analogy with the Ge(001) 2×1 reconstruction. The square symbols in Fig. 5 illustrate the dispersion of feature F with $k_{||}$. In view of these observations, feature F was assigned as a surface state.

The ARPES spectra (Fig. 2) of $AuIn_2$ are simpler than for $AuGa_2$. Four features, which arise from bulk valence-band transitions, are seen in the $AuIn_2$ case. The features labeled A correspond to transitions from an s-p band which crosses the Fermi level about halfway between Γ and X. The agreement between this experimental band and the Δ_1 band calculated by the interpolation scheme [Fig. 4(c)] is good, so the A feature is assigned to the valence band with Δ_1 symmetry. Within the uncertainty in the momentum, the experiment and the theory agree quite well as to the binding energy of the band at the X point, but the dispersion of the band is not in as good agreement.

Features B, C, and E in the $AuIn_2$ spectra result from transitions from d bands with the same symmetry as those observed for $AuGa_2$. These bands show even less dispersion between Γ and X than $AuGa_2$, presumably because the Au-Au separation is larger in $AuIn_2$ and the orbital interactions of the neighboring atoms is smaller. The agreement of the three experimental d bands with the interpolation scheme calculation is excellent over the entire region between Γ and X. $AuIn_2$ exhibits the same $(\sqrt{2}\times\sqrt{18})R45°$ reconstruction as $AuGa_2$, so it should not be surprising to find a similar surface state on the (001) surface of $AuIn_2$. Feature D in the $AuIn_2$ spectra (Fig. 2) shows the same behavior as feature F (Fig. 1) in the case of $AuGa_2$. It is more sensitive to surface contamination than any of the bulk features. It shows no dispersion for normal photoemission in the range of photon energies used in this experiment. However, feature D does disperse with $k_{||}$, as shown by the circles in Fig. 5. Therefore, this feature has also been assigned as a surface state.

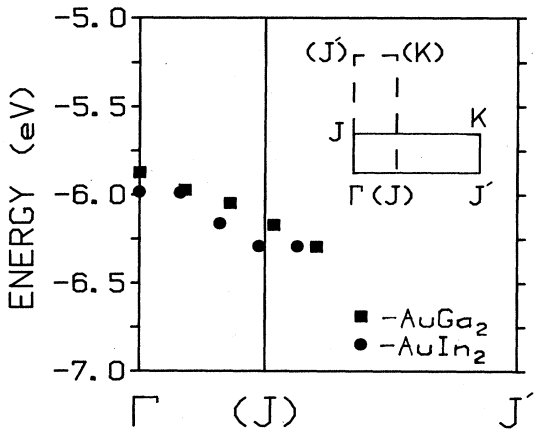

FIG. 5. Dispersion of the features assigned as surface states in $AuGa_2$ (squares) and $AuIn_2$ (circles) with $k_{||}$. Because the surface reconstruction consists of two perpendicular domains, $k_{||}$ varies simultaneously from Γ to J and Γ to J' (in the surface BZ) as the photoelectron emission angle is varied in the [110] azimuth. The two perpendicular surface BZ's are shown in the inset.

It would be possible to unambiguously map out both the valence and conduction bands of these two compounds using the triangulation technique of collecting ARPES spectra from two different surfaces.[25–27] If two features are seen at the same binding energy from two different surfaces, then the value of $\mathbf{k}$ can be determined absolutely. This would provide the necessary information for plotting the E versus $\mathbf{k}$ dispersion relations of both initial and final states without invoking a plane-wave final-state approximation. The resulting experimental energy bands could then be used in conjunction with the interpolation scheme to determine a truly experimental band structure.

V. CONCLUSIONS

The ARPES spectra of $AuGa_2$ and $AuIn_2$ are reasonably simple, and all features in both sets of spectra can be assigned to either bulk or surface transitions. Using a plane-wave final-state approximation, the d bands of both compounds are in good agreement with an interpolation scheme calculation, which was fitted to a first-principles APW calculation and adjusted to agree with the experimental results only at the Γ point of the BZ. The experimental s-p bands do not agree with the interpolation scheme as well as the d levels. However, the spectral features of the s-p bands are much broader, causing a larger uncertainty in the crystal momentum. The $AuGa_2$ spectra are somewhat more complicated than in $AuIn_2$, in that they contain features due to surface umklapp processes. Essentially identical surface states that reside in a

band gap between Γ_7^+ and the lower Γ_8^+ energy positions in the valence bands have been found on the (001) surfaces of $AuGa_2$ and $AuIn_2$.

Surprisingly, the splittings of the Au $5d$ bands at Γ for $AuGa_2$ and $AuIn_2$ are nearly identical with each other and with elemental Au, despite the large difference in the Au-Au distances in the three systems. A satisfactory explanation of this observation requires further experiments and/or detailed *ab initio* calculations. The difference observed in the total d-band width of the two compounds arises because the d bands of $AuIn_2$ disperse less than those of $AuGa_2$, whereas the d-band width of Au is also broadened by mixing of the d bands with a plane-wave state.

ACKNOWLEDGMENTS

The authors wish to thank R. J. Baughman of Sandia National Laboratories for supplying the $AuGa_2$ and $AuIn_2$ single crystals, and J. A. Yarmoff, T. C. Tsai, and R. Blumenthal for assistance with the experimental measurements. This work was performed at the Stanford Synchrotron Radiation Laboratory, which is supported by the U.S. Department of Energy under Grant No. DE-AC03-82ER13000, in cooperation with the Stanford Linear Accelerator Center. Support for this project was provided by the U.S. Office of Naval Research. R.S.W. acknowledges the Camille and Henry Dreyfus Foundation and the Alfred P. Sloan Foundation for support.

[1]S. S. Vishnubhatla and J. P. Jan, Philos. Mag. **16**, 45 (1967).
[2]J. T. Longo, P. A. Schroder, and D. J. Sellmeyer, Phys. Rev. **182**, 658 (1969).
[3]J. C. Abele, J. H. Brewer, and M. H. Halloran, Solid State Commun. **9**, 977 (1971).
[4]P. D. Chan and D. A. Shirley, in *Electronic Density of States*, edited by L. H. Bennet, Natl. Bur. Stand. (U.S.), Spec. Publ. No. 323 (U.S. GPO, Washington, D.C., 1971), p. 791.
[5]S. Hüfner, J. H. Wernick, and K. W. West, Solid State Commun. **10**, 1013 (1972).
[6]P. M. Th.M. van Attekum, G. K. Wertheim, G. Crecelius, and J. H. Wernick, Phys. Rev. B **22**, 3998 (1980).
[7]J. G. Nelson, J. R. Lince, W. J. Gignac, and R. S. Williams, J. Vac. Sci. Technol. A **2**, 534 (1984).
[8]G. V. Hansson and S. A. Flodström, Phys. Rev. B **17**, 473 (1978).
[9]J. Stöhr, P. S. Wehner, R. S. Williams, G. Apai, and D. A. Shirley, Phys. Rev. B **17**, 587 (1978).
[10]P. S. Wehner, R. S. Williams, S. D. Kevan, D. Denley, and D. A. Shirley, Phys. Rev. B **19**, 6164 (1979).
[11]A. C. Switendick and A. Narath, Phys. Rev. Lett. **22**, 1423 (1969).
[12]S. Kim, J. G. Nelson, and R. S. Williams, preceding paper [Phys. Rev. B **31**, 3460 (1985)].
[13]The $AuGa_2$ and $AuIn_2$ crystals used in this experiment were pieces from larger ingots which were grown by R. J. Baughman of Sandia National Laboratories, Albuquerque, New Mexico. For details of the growth of the crystals, see R. J. Baughman, Mater. Res. Bull. **7**, 505 (1972).
[14]G. D. Mahan, Phys. Rev. B **2**, 4334 (1970).
[15]R. S. Williams, P. S. Wehner, J. Stöhr, and D. A. Shirley, Phys. Rev. Lett. **39**, 302 (1977).
[16]P. J. Feibelman, Surf. Sci. **46**, 558 (1974).
[17]M. P. Seah and W. A. Dench, Surf. Interface Anal. **1**, 2 (1979).
[18]J. A. Raynes, Phys. Lett. **7**, 114 (1963).
[19]C. J. Ballhausen, *Introduction to Ligand Field Theory* (McGraw-Hill, New York, 1962), p. 118.
[20]K. A. Mills, R. F. Davis, S. D. Kevan, G. Thorton, and D. A. Shirley, Phys. Rev. B **22**, 581 (1980).
[21]Richard F. Davis, Ph.D. thesis, University of California, Berkeley, 1981.
[22]H. Eckhardt, L. Fritsche, and J. Noffe, J. Phys. F **14**, 97 (1984).
[23]J. C. Slater and G. F. Koster, Phys. Rev. **94**, 1498 (1954).
[24]J. Hermanson, Solid State Commun. **22**, 9 (1977).
[25]E. O. Kane, Phys. Rev. Lett. **12**, 97 (1964).
[26]H. Neddermeyer, Solid State Commun. **40**, 809 (1981).
[27]M. Pessa, M. Lindross, H. Asonen, and N. V. Smith, Phys. Rev. B **25**, 738 (1982).